Short-wave infrared barriode detectors using InGaAsSb absorption material lattice matched to GaSb

A. P. Craig, M. Jain, G. Wicks, T. Golding, K. Hossain, K. McEwan, C. Howle, B. Percy, and A. R. J. Marshall

---

Articles you may be interested in

Demonstration of high performance bias-selectable dual-band short-/mid-wavelength infrared photodetectors based on type-II InAs/GaSb/AlSb superlattices
Appl. Phys. Lett. **102**, 011108 (2013); 10.1063/1.4773593

High operating temperature interband cascade midwave infrared detector based on type-II InAs/GaSb strained layer superlattice
Appl. Phys. Lett. **101**, 021106 (2012); 10.1063/1.4733660

Performance improvement of longwave infrared photodetector based on type-II InAs/GaSb superlattices using unipolar current blocking layers
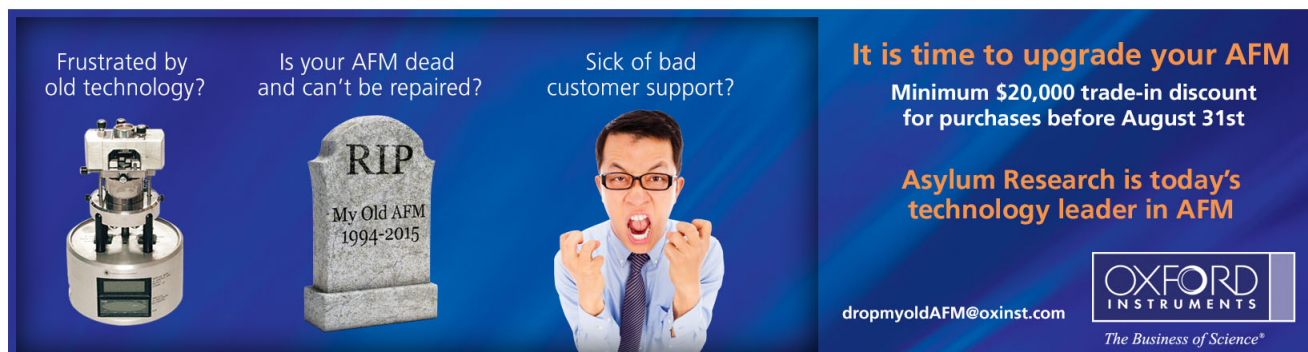Appl. Phys. Lett. **96**, 231107 (2010); 10.1063/1.3446967

Extended wavelength InGaAs on GaAs using InAlAs buffer for back-side-illuminated short-wave infrared detectors
Appl. Phys. Lett. **82**, 2838 (2003); 10.1063/1.1569042

InGaAsSb thermophotovoltaic diode: Physics evaluation
J. Appl. Phys. **85**, 2247 (1999); 10.1063/1.369533

Short-wave infrared barriode detectors using InGaAsSb absorption material lattice matched to GaSb

A. P. Craig,[1] M. Jain,[2] G. Wicks,[3] T. Golding,[2,3] K. Hossain,[3] K. McEwan,[4] C. Howle,[4] B. Percy,[1] and A. R. J. Marshall[1]

[1]*Physics Department, Lancaster University, Lancaster LA1 4YB, United Kingdom*
[2]*Amethyst Research Ltd., Kelvin Campus, West of Scotland Science Park, Glasgow G20 0SP, United Kingdom*
[3]*Amethyst Research, Inc., 123 Case Circle, Ardmore, Oklahoma 73401, USA*
[4]*Defence Science and Technology Laboratory, Porton Down, Salisbury, Wiltshire SP4 0JQ, United Kingdom*

Short-wave infrared barriode detectors were grown by molecular beam epitaxy. An absorption layer composition of $In_{0.28}Ga_{0.72}As_{0.25}Sb_{0.75}$ allowed for lattice matching to GaSb and cut-off wavelengths of 2.9 μm at 250 K and 3.0 μm at room temperature. Arrhenius plots of the dark current density showed diffusion limited dark currents approaching those expected for optimized HgCdTe-based detectors. Specific detectivity figures of around 7×10^{10} Jones and 1×10^{10} Jones were calculated, for 240 K and room temperature, respectively. Significantly, these devices could support focal plane arrays working at higher operating temperatures. © *2015 Author(s). All article content, except where otherwise noted, is licensed under a Creative Commons Attribution 3.0 Unported License.* [http://dx.doi.org/10.1063/1.4921468]

Barrier infrared detectors working in the 3–5 μm spectral range have been studied extensively in recent years. These were based upon absorption layers of InAs,[1] InAsSb,[2,3] or strained-layer-superlattices.[4,5] While focal plane arrays (FPAs) for thermal-vision cameras are the primary application for such devices, the spectral fingerprints of various pollutant gasses, including methane (3.3 μm), CO_2 (4.6 μm), and CO (4.2 μm),[6] further allow for their detection—particularly for environmental or pollution monitoring. This work presents an extension of the barrier infrared detector design to the short wave infrared (SWIR) region between 1 and 3 μm; this particularly offers the potential for detection of various chemical, biological, or explosive (e.g., TNT or RDX) "threat agents."[7] Previously, detectors for the SWIR spectral range were based upon HgCdTe[8] or lattice-mismatched InGaAs on InP.[9] However, the procedures used to grow HgCdTe material are typically confidential, hindering development. Weak bond strength (fragility) and control of mole fraction are also of concern. Furthermore, InGaAs on InP devices suffer from low material quality, i.e., threading dislocations which occur due to the lattice mismatch, with implications for device dark current performance. The devices presented in this work differ from existing *nBn* detectors through optimization for SWIR applications, providing superior specific detectivity (D*) for the same temperature of operation when compared to existing *nBn* detectors (when operated at SWIR wavelengths). This optimization was achieved by using an $In_{0.28}Ga_{0.72}As_{0.25}Sb_{0.75}$ absorption layer in order to reduce device dark currents: the quaternary system allows for a wider bandgap than InAs(Sb). The choice of a different absorption material—with different band offsets—then necessitates a redesigned barrier layer, which was implemented using an AlGaSb alloy. The $In_{0.28}Ga_{0.72}As_{0.25}Sb_{0.75}$ alloy composition was chosen to allow for a cut-off wavelength in the SWIR whilst maintaining a lattice constant matched to the GaSb substrate. Dark current performance was found to approach predicted levels for optimized HgCdTe based devices, via Rule 07.[10] Through spectral response measurements, the cut-off wavelength was determined to be around 2.9 μm at 250 K and 3.0 μm at room temperature. D* figures of 7×10^{10} Jones and 1×10^{10} Jones were calculated, at 240 K and room temperature, respectively.

Growth was performed by solid-source molecular beam epitaxy (MBE). Processing was performed using a citric-acid-based etchant and Ti/Au metallizations. Mesas were defined by etching down to, but not through, the barrier layer. An AlSb etch stop layer was used. The ground contact was made by etching through the absorption layer to a depth of ~600 nm. X-ray diffraction (XRD) measurements were carried out using a Bede QC200 diffractometer. Dark current measurements were carried out using a Lakeshore TTPX low-temperature probe station and Keithley 2400 and 6430 Sourcemeters®. Spectral response was carried out using a 900 °C blackbody source, a Bentham TMc300 monochromator and a Stanford SR830 lock-in amplifier. The spectra were normalized using a pyroelectric detector from Judson. 4–300 K photoluminescence (PL) measurements were carried out using a 514 nm wavelength Ar-ion laser and an Oxford Instrument continuous flow He cryostat with CaF_2 optics.

The epilayer structure is shown in Figure 1. Compositional information was confirmed through XRD measurements. A single peak for the absorption layer and substrate confirmed that the absorption and contact layers were lattice matched to GaSb. The width of the peak was 52 arc sec, confirming good quality layer growth. A second peak due to the barrier layer was noted, displaced from the absorption layer peak by ~475 arc sec. Based upon the fitted composition of the barrier layer, the 60 nm layer thickness was lower than the critical thickness predicted by the model of Matthews and Blakeslee[11] (61 nm), confirming strained layer growth. Band

FIG. 1. Epilayer structure, with compositional, doping, and thickness information. The AlGaSb layer is the barrier.

FIG. 3. Photoluminescence results between 4 and 300 K. Features due to water vapour absorption around 2.7 μm were excluded when performing fittings to determine the bandgap.

alignments—as calculated using the strain-dependent model of Krijn[12]—are shown in Figure 2. It can be seen that there is a conduction band barrier of around 0.8 eV, suppressing the flow of dark currents due to majority carriers, but a valence band offset as small as 0.025 eV, allowing the flow of photo-generated holes. Using the bowing parameter—for InGaAsSb lattice matched to GaSb—suggested by Meyer,[13] the bandgap of the absorption layer was calculated to be 0.53 eV and 0.45 eV, at 4 K and room temperature, respectively. However, PL measurements, as shown in Figure 3, indicated notable variation from this theory. Fittings were made to single Gaussian functions, with the region around 2.7 μm excluded to avoid interference from the effects of water vapor absorption. The measured bandgap was 0.462 eV and 0.435 eV, at 4 K and room temperature, respectively. Though it is possible that the freezing out of dopant impurities can affect the PL peak position at low temperatures, i.e., Moss-Burstein shift is negated, the difference ($\sim$70 meV) seems to be too large for this to be the cause of the discrepancy. Reference 13 states that the bowing parameter recommended (0.75 eV) is based on a composite of all available experimental results. However, the studies listed were noted to be based on alloy compositions relatively close to binary InAs or GaSb, whereas the composition of the layers in this work is close to the miscibility gap, i.e., somewhere in between. Given the lack of data available in the literature for compositions close to $In_{0.28}Ga_{0.72}As_{0.25}Sb_{0.75}$, it was felt that the apparent contradiction likely indicates a real variation from the bowing parameter in Ref. 13. A Varshni fitting was made to determine the temperature dependence of the energy gap, based upon the PL
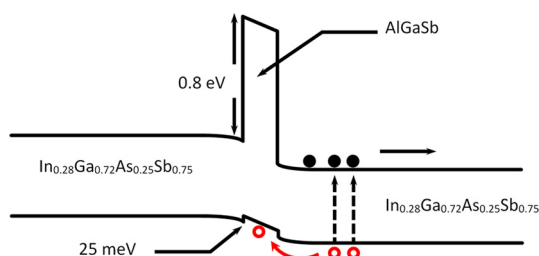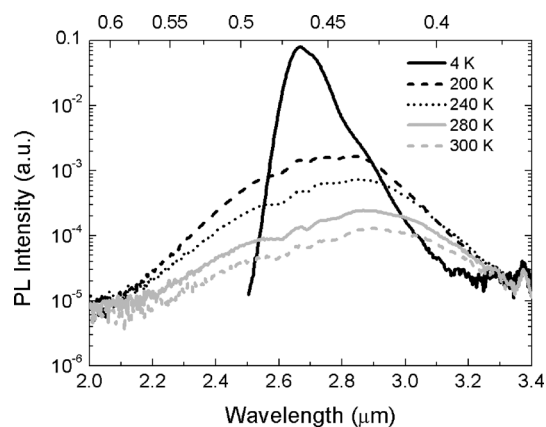
measurements at temperatures between 4 and 300 K. The Varshni parameters were determined to be $E_g(0K) = 0.47$ eV, $\alpha = 5.3 \times 10^{-4}$ eVK^{-1} and $\beta = 1076$ K. Figure 4 further shows normalized spectral response results, indicating a cut off wavelength of around 2.9 μm at 250 K (0.432 eV) and 3.0 μm (0.419 eV) at room temperature. These values were obtained by plotting the square of the photoresponse against energy, fitting the low energy region, and extrapolating to zero.

Figure 5 shows Arrhenius plots of the dark current density, as measured using a Keithley 2400 Sourcemeter. A Keithley 6430 "Sub-Femtoamp" Sourcemeter was also used to lower the noise floor, allowing for measurements to be taken below 200 K. The Keithley 2400 Sourcemeter has a shorter integration time, and hence was preferred for measurements at higher temperatures, where the currents measured significant exceeded its noise floor. The activation energy fitting shown yielded a result of 0.41 eV, which is close to the low temperature bandgap quoted from PL ($\Delta \sim 50$ meV). This correspondence indicates that the dark currents are diffusion limited at temperatures down to 175 K, and that any residual valence band barrier between the absorption and barrier layers, e.g., due to band bending, is small. On the other hand, Shockley-Read-Hall (SRH) limited dark currents are known to result in activation energies of around half the bandgap, whereas surface limited devices typically show weak temperature dependence. Therefore,

FIG. 2. Modeled bandstructure, following the model of Krijn,[12] using the fitted XRD parameters shown in Figure 1.
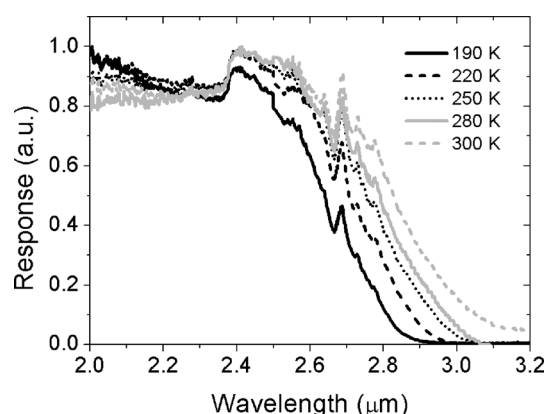

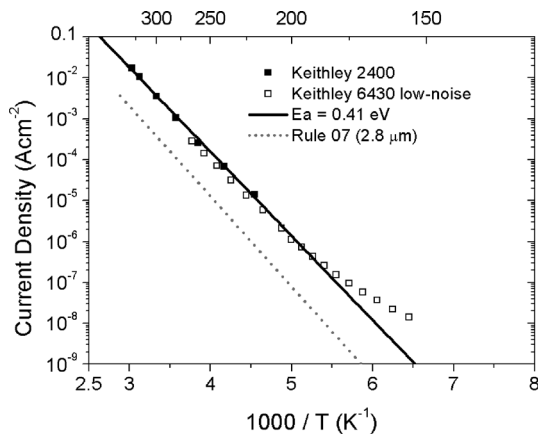FIG. 4. Normalized spectral response data, between 190 and 300 K.

FIG. 5. Dark currents as a function of temperature, as measured using Keithley 2400 and 6430 Sourcemeters, an activation energy fitting, and a line from Rule 07. The bias voltage was −0.1 V.

FIG. 7. Dark currents as a function of bias (left) and quantum efficiency (right) as measured using a fiber-coupled 1.55 μm laser.

diffusion current was identified as the dominant dark current source, confirming the suppression of SRH and surface currents by the barrier design. Figure 5 further shows a line calculated using Rule 07 for a cut-off wavelength of 2.9 μm (corresponding to the 50% cut-off wavelength of our devices). Rule 07 is intended to indicate the expected performance of an optimized HgCdTe device, and was created through an empirical fitting of the dark current performance of HgCdTe detectors with cut-off wavelengths between 2.5 and 15.6 μm.[10] Specific detectivity data was calculated next using responsivity measurements made using a fiber-coupled 1.55 μm laser, calibrated using an Oriel power meter. The results were based on shielded dark current measurements and are shown in Figure 6. It can be seen that the behavior is approximately independent of bias, as a result of dark currents which are also approximately bias independent, as shown in Figure 7. It can further be seen that D* increases with bias at 300 K, but decreases with bias at lower temperatures. This is due to smaller gradients in the dark currents for higher temperatures, as shown in Figure 7, so that the increase in responsivity at higher bias conditions becomes less significant. These figures can be compared with state-of-the art HgCdTe-based sensors available commercially, e.g., those of Ref. 14 which have a 3 μm cut-off wavelength and D* figures of around 3×10^{11} Jones for 195 K operating

temperature. For a more complete consideration, it should be noted that our devices did not have an antireflection coating, and that our D* figures were obtained using a 1.55 μm laser. Since D* depends on the photon energy, an improvement by a factor of ~1.7 would be expected close to the 2.7 μm cut-off wavelength. Quantum efficiency (QE) was measured to be approximately 30% for small applied bias (at 300 K). The measurement was carried out for top-injection and single pass conditions. The QE was further found to be approximately temperature insensitive. The bias dependence of the QE likely results from the lowering of a small residual potential barrier between the absorption and barrier layers. Figure 8 shows the temperature dependence of the hole diffusion length, as inferred from the area dependence of the dark currents using a fitting procedure.[15] Square mesas with side lengths of 25 μm, 50 μm, 100 μm, and 200 μm were treated using an effective area approximation including a term representing a rounded profile at the device corners. As illustrated in the inset, the maximum diffusion length at 220 K is around 35 μm. FPAs may require cross-talk between adjacent devices to be suppressed; one way to achieve this could be through heavy *n*-type doping of the absorption layer. Careful optimization of the doping level would be required, however, since increased doping will result in lower diffusion lengths for minority carriers. Deep-etched mesa processing (where the barrier layer is etched when defining the mesas) could also be used to remove cross-talk, but this could result in the reintroduction of some level of surface currents. Figure 9
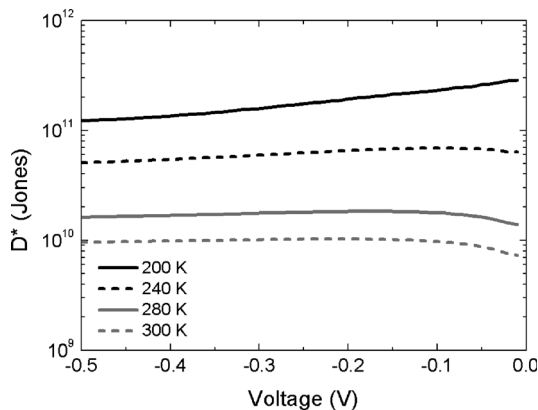

FIG. 6. Specific detectivity, as a function of bias and temperature. Weak bias dependence is observed as a result of somewhat bias-independent dark currents.
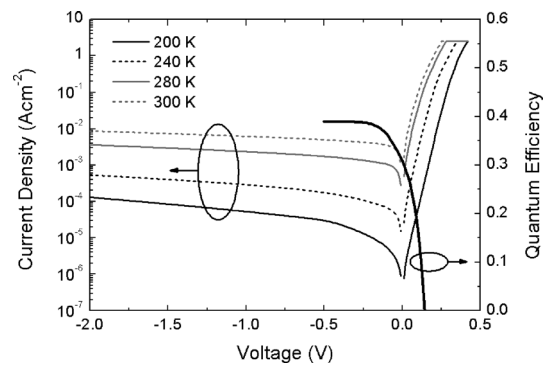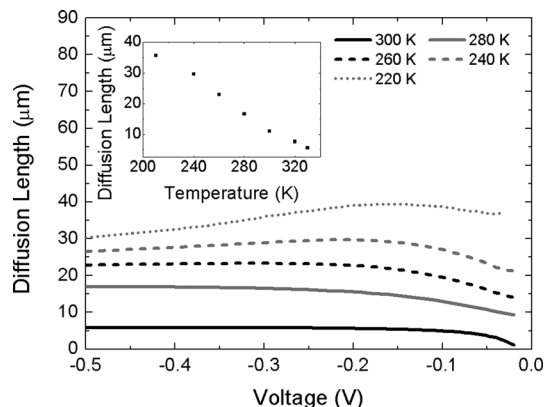

FIG. 8. Temperature dependence of the hole diffusion length, as established from the dark currents using a fitting procedure.
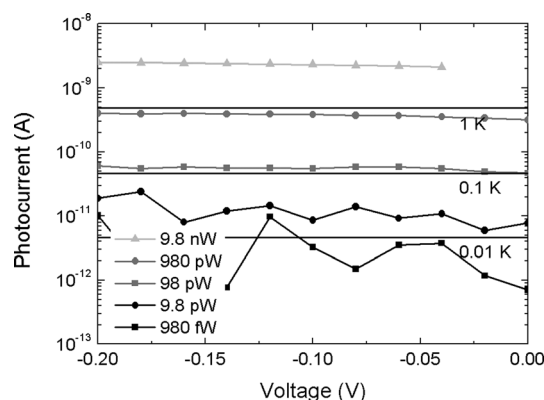
FIG. 9. Photocurrents for 200 μm side-length (square) mesas, measured under low excitation powers, as provided by attenuating a 1.55 μm laser. The horizontal lines indicate the magnitude of the dark current shift with the corresponding change in device temperature.

shows photocurrent measurements at 220 K for low excitation powers, as obtained by attenuating the 1.55 μm laser. As illustrated, signal powers as small as 980 fW were resolved. All photocurrents were established using a DC measurement technique, i.e., no phase sensitive detection was necessary. Using the known temperature dependence of the dark currents—from Fig. 5—lines representing the shift expected due to a given change in device temperature are also plotted. It can be seen that any small fluctuations in the device temperature could become significant when the smallest signal powers are measured. The smallest signal powers resolved can be compared with the minimum noise level, i.e., the sum of Shot noise and thermal noise, which is 5×10^{-14} A Hz$^{-1/2}$ at 220 K.

In summary, an SWIR "barriode" detector structure was demonstrated based on quaternary InGaAsSb absorption material and a ternary AlGaSb barrier layer. The structure was grown lattice matched to GaSb. Diffusion limited dark currents and a level of performance approaching that predicted by Rule 07 were demonstrated. Spectral response measurements revealed cut off wavelengths of 2.9 μm at 250 K and 3.0 μm at room temperature. At 240 K, D* values of around 7×10^{10} Jones were calculated for -0.1 V bias voltage. Significantly, these devices could support focal plane arrays working at higher operating temperatures.

[1]S. Maimon and G. W. Wicks, Appl. Phys. Lett. **89**, 151109 (2006).
[2]A. P. Craig, A. R. J. Marshall, Z.-B. Tian, S. Krishna, and A. Krier, Appl. Phys. Lett. **103**, 253502 (2013).
[3]A. Soibel, C. J. Hill, S. A. Keo, L. Hoglund, R. Rosenberg, R. Kowalczyk, A. Khoshakhlagh, A. Fisher, D. Z.-Y. Ting, and S. D. Gunapala, Appl. Phys. Lett. **105**, 023512 (2014).
[4]G. Bishop, E. Plis, J. B. Rodriguez, Y. D. Sharma, L. R. Dawson, and S. Krishna, J. Vac. Sci. Technol., B **26**(3), 1145 (2008).
[5]J. B. Rodriguez, E. Plis, G. Bishop, Y. D. Sharma, H. Kim, L. R. Dawson, and S. Krishna, Appl. Phys. Lett. **91**, 043514 (2007).
[6]A. Krier, M. Yin, V. Smirnov, P. Batty, P. J. Carrington, V. Solovev, and V. Sherstnev, Phys. Status Solidi A **205**(1), 129–143 (2008).
[7]M. Jain, G. Wicks, A. Marshall, A. Craig, T. Golding, K. Hossain, K. McEwan, and C. Howle, Proc. SPIE **9073**, 907304 (2014).
[8]A. Rogalski, "Infrared detectors: Status and trends," Prog. Quantum Electron. **27**, 59–210 (2003).
[9]H. W. Yoon, M. C. Dopkiss, and G. P. Eppeldauer, Proc. SPIE **6297**, 629703 (2006).
[10]W. E. Tennant, D. Lee, M. Zandian, E. Piquette, and M. Carmody, J. Electron. Mater. **37**, 1406–1410 (2008).
[11]J. W. Matthews and A. E. Blakeslee, J. Cryst. Growth **27**, 118 (1974).
[12]M. P. C. M. Krijn, Semicond. Sci. Technol. **6**, 27 (1991).
[13]I. Vurgaftman, J. R. Meyer, and L. R. Ram-Mohan, J. Appl. Phys. **89**, 5815 (2001).
[14]Vigo System S.A., "PV-4TE Series" (2015).
[15]E. A. Plis, S. Myers, M. N. Cutty, J. Malifert, E. P. Smith, S. Johnson, and S. Krishna, Proc. SPIE **7945**, 79451R (2011).